International Journal of Nanomedicine

Dovepress

open access to scientific and medical research

Open Access Full Text Article

ORIGINAL RESEARCH

Neoadjuvant Gold Nanoshell-Based Photothermal Therapy Combined with Liposomal Doxorubicin in a Mouse Model of Colorectal Cancer

Marina Simón[1,*], Jesper Tranekjær Jørgensen[1,*], Kamilla Norregaard[1], Jonas Rosager Henriksen[2], Gael Clergeaud[2], Thomas L Andresen[2], Anders Elias Hansen[2], Andreas Kjaer[1]

[1]Department of Clinical Physiology and Nuclear Medicine & Cluster for Molecular Imaging, Copenhagen University Hospital – Rigshospitalet & Department of Biomedical Sciences, University of Copenhagen, Copenhagen, Denmark; [2]Department of Health Technology, Section for Biotherapeutic Engineering and Drug Targeting, Technical University of Denmark, Kongens Lyngby, Denmark

*These authors contributed equally to this work

Correspondence: Andreas Kjaer, Department of Clinical Physiology and Nuclear Medicine & Cluster for Molecular Imaging, Copenhagen University Hospital – Rigshospitalet & Department of Biomedical Sciences, University of Copenhagen, Copenhagen, Denmark, Email akjaer@sund.ku.dk

Introduction: Traditional cancer treatments, such as chemotherapy, are often incapable of achieving complete responses as standalone therapies. Hence, current treatment strategies typically rely on a combination of several approaches. Nanoparticle-based photothermal therapy (PTT) is a technique used to kill cancer cells through localized, severe hyperthermia that has shown promise as an add-on treatment to multiple cancer therapies. Here, we evaluated whether the combination of gold nanoshell (NS)-based PTT and liposomal doxorubicin could improve outcome in a mouse model of colorectal cancer.

Methods: First, NS-based PTT was performed on tumor-bearing mice. Radiolabeled liposomes were then injected at different timepoints to follow their accumulation in the tumor and determine the ideal injection time after PTT. In addition, fluorescent liposomes were used to observe the liposomal distribution in the tumor after PTT. Finally, we combined PTT and doxorubicin-loaded liposomes and studied the effect of the treatment strategy on the mice by following tumor growth and survival.

Results: PTT significantly improved liposomal accumulation in the tumor, but only when the liposomes were injected immediately after the therapy. The liposomes accumulated mostly in regions adjacent to the ablated areas. When PTT was combined with liposomal doxorubicin, the mice experienced a slowdown in tumor growth and an improvement in survival.

Conclusion: According to our preclinical study, NS-based PTT seems promising as an add-on treatment for liposomal chemotherapy and potentially other systemic therapies, and could be relevant for future application in a clinical setting.

Keywords: liposomes, PET imaging, chemotherapy, hyperthermia, gold nanoparticles

Introduction

The approach of combining standard cancer therapeutics to overcome the limitations of each individual treatment has been a focus of scientific research for years.[1,2] Traditional anti-cancer therapies like chemo- and radiotherapy are highly efficient for certain tumor types, but recurrence is still a common issue, as well as the side effects caused by these treatments.[3]

Different delivery systems have been developed to overcome rapid clearance, toxicity, and low intracellular absorption when administering therapeutic agents, with the aim of improving drug distribution.[4] Liposomes have shown promise due to some unique properties, such as biodegradability, biocompatibility, hydrophobic and hydrophilic character, and low toxicity in the body.[5] In addition, liposomes can passively reach and accumulate in tumors through the enhanced permeability and retention (EPR) effect, from where they can release the drug in a slow and controlled manner.[6]

Received: 9 September 2022
Accepted: 23 December 2022
Published: 17 February 2023

Graphical Abstract

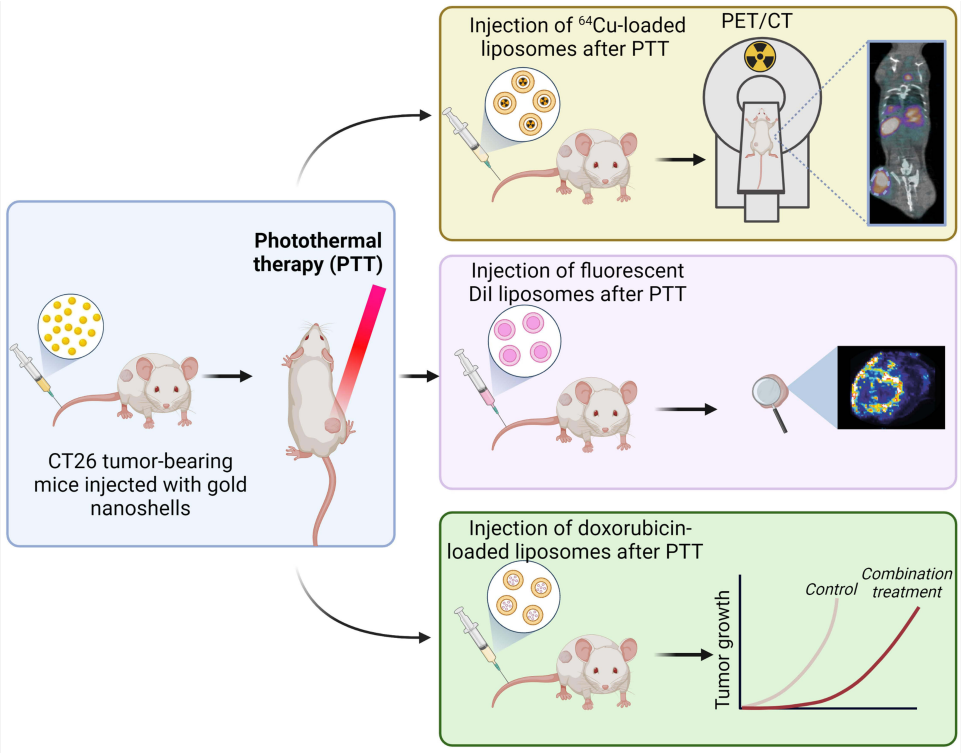

Photothermal therapy (PTT), a minimally invasive technique for the ablation of solid tumors through local hyperthermia, has shown great potential due to its ability to cause tumor death while sparing surrounding healthy tissues.[7–10] The method relies on light-absorbing nanoparticles, such as gold nanoshells (NS), which are injected into the patient and accumulate in the tumor. When the tumors are irradiated with a source of near-infrared (NIR) light, the nanoparticles transform this light into heat, causing irreversible damage to the malignant cells.[11,12] The NS present high photothermal efficiency and have shown to be biocompatible and non-toxic, making them ideal for PTT.[13,14] In fact, NS-based PTT has already been tested in clinical trials with promising results.[15,16]

However, PTT applied as monotherapy is often not sufficient to eradicate an entire tumor mass. Limited drug penetration of photothermal agents and insufficient penetration depth of NIR light play an important part in the incomplete responses, often leading to an ablation zone with surrounding heat dissipation towards the periphery of the tumor.[17] Nonetheless, hyperthermia can also lead to an increase in blood flow, favoring the extravasation of macromolecules.[18] Therefore, combining PTT with other systemic cancer treatments could be a promising approach.[19] In accordance with this idea, the combination of laser treatment with chemotherapy has shown to be able to potentiate the effect of the chemotherapeutic drugs.[20] Studies have proven that DNA damaging agents, such as doxorubicin (DOX), are more effective when combined with hyperthermia since DNA repair is temperature-dependent.[21–23] In fact, Caelyx®/Doxil®, a polyethylene glycosylated (PEGylated) liposomal formulation of DOX, is FDA-approved for multiple indications.[24] It has been shown that liposomal encapsulation limits toxicity and improves DOX delivery to the tumor. The high temperatures induced by PTT could further enhance this drug delivery. Taken together, a combined effect of PTT and a chemotherapeutic agent could reduce drug resistance (drug concentrations used in combination therapy are usually lower than for chemotherapy alone), increase drug delivery towards the tumor (due to the increased perfusion), and improve treatment outcome.[22]

In this study, we investigated the potential of NS-based PTT to enhance the liposomal delivery to solid tumors, with the aim of improving treatment outcome when applying PTT in combination with the administration of DOX-loaded PEGylated liposomes (Caelyx®). Radiolabeled and fluorescent PEGylated liposomes were used to study the biodistribution after PTT in mice bearing CT26 (colorectal carcinoma) tumors. In addition, PTT was applied as neoadjuvant to DOX-loaded liposomes and the treatment response was monitored by measuring changes in tumor volume and survival (humane endpoints).

Materials and Methods

Gold Nanoshells

The gold nanoparticles used in this study were 800 nm Resonant BioPure^{TM} Gold NS (NanoComposix, USA). The total diameter of the particles was 157 ± 9 nm and the diameter of the silica core was 119 nm ± 5 nm. Shell thickness was 19 nm. The NS were functionalized with 5 kDa methoxy polyethylene glycol and the zeta potential was −42 mV (reported by the supplier).

Preparation of ^{64}Cu-Loaded Liposomes

Remote loading of $^{64}Cu^{2+}$ into stealth® liposomes (HSPC: Chol: DSPE-PEG2k in the molar ratio 56.5:38.2:5.3) was done as previously described.[20] Briefly, 2.2 mL 6.6 mM stealth® liposomes were added to 650 MBq dried $^{64}CuCl_2$ and stirred at 55 °C for 75 minutes. The labeling efficiency and fraction of free $^{64}Cu^{2+}$ were characterized using PD10 column separation and Radio-TLC.[21] The activity at the time of injection was set to 100 MBq/mL and the loading amounted to 95% (PD10 column). No detectable ^{64}Cu was identified using Radio-TLC. The liposomes had an average size of 105 nm and a polydispersity index of 0.03 as determined by dynamic light scattering.

The zeta-potential of stealth liposomes has previously been reported.[25,26]

Preparation of Fluorophore-Labeled Liposomes

Lipid constituents were dissolved in tertbutanol: water (1:1) at 70 °C and mixed at the following mol ratio, HSPC: Chol: DSPE-PEG2k: DiI (56.8:38:5:0.2 mol%), including DiI as a fluorescent membrane dye. The solution was snap-frozen in liquid nitrogen and freeze-dried overnight. The resulting lipid powder was hydrated for 1 hour at 70 °C in Hepes buffer (HBS, 10mM Hepes, 150mM NaCl, pH 7.4) to a final lipid concentration of 50 mM. Then, the lipid suspension was subsequently downsized by extruding 10-times through two stacked 100 nm polycarbonate membranes on a pressure extruder (Avanti, US). The resulting liposomes were stored at 4 °C overnight before characterization. The lipid concentration was 44.4 mM as quantified by inductively coupled plasma mass spectrometry, and the size and polydispersity of the particles were 103 nm and 0.022 as determined by dynamic light scattering.

Cell Line and Animal Model

The animal experiments were approved by the Danish Animal Experimentation Council and undertaken in compliance with the directive 2010/63/EU of the EU legislation on the protection of animals used for scientific purposes.

The animals used in this study were five to six-week-old BALB/cJRj female mice from Janvier Labs (Le Genest Saint Isle, France). Mice were allowed to acclimatize for a week after arrival, with access to water and food ad libitum. For tumor implantation, CT26 cells (ATCC) were first cultured in RPMI 1640 + GlutaMAX medium with 10% fetal bovine serum and 1% penicillin-streptomycin (Thermo Fisher Scientific) at 37 °C and in 5% CO_2. When they reached ~70% confluence, 3×10^5 cells (in 0.1 mL PBS) were injected into the left flank of the mice. The mice were anesthetized during the inoculation process by breathing 4% sevoflurane (Abbott Scandinavia AB, Sweden). Tumor size was measured with the use of a caliper and the tumor volume was determined following the formula: volume = ½ (length × width^2). When tumors reached ~1000 mm^3 animals were euthanized. The study was terminated on day 60.

Photothermal Therapy in vivo

The day before PTT, mice were injected with 190 µL of NS (5 x 10^{10} particles/mL) intravenously. The following day, mice were anesthetized and placed on a heating pad under an 807-nm diode laser beam, with a beam diameter of ~1 cm. Mice were irradiated at a laser intensity of 1.5 W/cm^2 for five minutes. During irradiation, the maximum temperatures on the tumor surface were recorded every 30 seconds using a thermographic camera (FLIRT420 Infrared Camera, FLIR systems, Täby, Sweden). The images were analyzed within the FLIR Thermal Studio software. Mice were given buprenorphine as pain relief before PTT and every 6 to 8 hours for the next 24 hours.

In vivo Distribution of ^{64}Cu-Loaded Liposomes Through Positron Emission Tomography/Computed Tomography

Positron emission tomography with computed tomography (PET/CT) was used to study the distribution of ^{64}Cu-loaded liposomes in mice bearing CT26 tumors. Animals were divided into four groups (n = 5 per group). The first three groups underwent PTT and were injected intravenously with ~10 MBq of ^{64}Cu-loaded liposomes immediately after PTT (0 h group), 6 hours (6 h group), or 24 hours (24 h group) after therapy. The fourth group received ^{64}Cu-loaded liposomes but no PTT (Control group). Animals were then PET/CT scanned 10 minutes and 24 hours after liposome injection. For this, mice were anesthetized and placed in a small animal PET/CT scanner (preclinical PET/CT Inveon, Siemens Medical Solutions, Malvern, PA, USA). CT scans were acquired using 360 projections, 65 kV voltage, 500 µA current, and 450 ms of exposure. PET scans were acquired with an energy window set to 350–650 KeV and a timing window of 6 ns. Acquired datasets were reconstructed using maximum a posteriori (MAP) algorithm and CT-based attenuation correction. PET and CT images were co-registered and analyzed within the Inveon Research Workstation software (Siemens Preclinical solutions). Regions of interest (ROIs) were manually drawn on whole tumor regions and uptake was quantified as the mean percent injected dose per gram of tissue (%ID/g).

Fluorescence Imaging and Histological Analysis

Mice (n = 3) were treated with PTT and subsequently injected with 100 µL DiI liposomes (16 mg/mL of lipid concentration) to observe the distribution of the liposomes in the tumor through fluorescent signal. Three extra mice were injected with the DiI liposomes without undergoing PTT. Mice undergoing PTT but no liposomal injection were also included as controls to observe the unspecific fluorescent signal. Animals were euthanized a day after liposomal injection and tumors were excised for ex vivo analysis. First, tumors were fixated in 4% paraformaldehyde followed by 25% sucrose for cryopreservation. Afterwards, they were embedded in an OCT-filled small container and frozen by placing the bottom of the container in a cold 2-methylbutane solution. Subsequently, they were cut into 4 and 20 µm slices on a cryostat (Leica CM 1860, Leica Biosystems) and placed on glass slides. The 4 µm slides were kept at −80 °C for future histological analysis meanwhile representative 20 µm slides were used to observe DiI fluorescence on the Amersham Typhoon Biomolecular Imager (GE Healthcare). Typhoon images were analyzed within the Image Quant software.

To detect DiI fluorescence at a cellular level, 4 µm slides were fixated in 4 °C acetone and then stained with Hoechst 33,342 nucleic acid stain (1:5000 in PBS). Sections were scanned on Zeiss Axio Scan.Z1.

For hematoxylin and eosin (HE), Ki-67, and CD31 staining, 4 µm tissue slides were brought to room temperature, placed in 4 °C acetone, and afterwards in Histo-Clear solution. For HE, slides were stained with hematoxylin for 5 minutes, rinsed in water, and stained with eosin for 3 minutes.

For Ki-67 and CD31 staining, tissue slides underwent heat-induced epitope retrieval. This was done by covering the slides with either citrate buffer (pH = 6) for Ki-67 or Tris Buffer (pH = 9) for CD31 and placing them in a microwave for 15 minutes at 100 °C. The slides were then left to equilibrate to room temperature and rinsed in running water. Following, the slides were submerged in phosphate-buffered saline with KCl (K-PBS) + 0.1% tween 20 for five minutes and afterwards transferred to TBS. Slides were placed in Shandon racks and blocked with peroxidase-blocking Solution (S2023, Dako, Glostrup, Denmark) for 10 minutes, and then with bovine serum albumin, BSA, (2% BSA in K-PBS, A79096, Sigma Aldrich, St. Louis, MO, USA) for 20 minutes. Primary antibodies were diluted in BSA and incubated for

one hour at room temperature. The antibodies used were Anti-CD31 (1:50; ab28364, Abcam, Cambridge, UK) and Anti-Ki-67 (1:100; ab15580, Abcam). Next, the slides were incubated with horseradish peroxidase (HRP)-labeled polymer conjugated to secondary antibody (EnVision™ + System-HRP Labeled Polymer, Dako) anti-rabbit for 40 minutes. This was followed by incubation with DAB (Liquid DAB+ Substrate Chromogen System™, Dako) for six minutes. The sections were subsequently counterstained with Mayers hematoxylin (Region Hovedstadens Apotek, 854,183) for one minute. The slides were mounted using an automated glass coverslipper (Dako). Sections were scanned on Zeiss Axio Scan.Z1.

Combination Treatment

The day before treatment (day −1), CT26 tumor-bearing mice were divided into six groups with matching tumor size; PTT group (animals receiving PTT alone, mean tumor size on day −1 = 143.1 ± 18.3 mm^3; n = 16), DOX group (animals receiving free DOX, mean tumor size on day −1 = 140.2 ± 20.5 mm^3; n = 15), LIP group (animals receiving DOX-loaded liposomes, mean tumor size on day −1 = 145.2 ± 19.9 mm^3; n = 15), PTT + LIP group (animals receiving PTT and DOX-loaded liposomes, mean tumor size on day −1 = 138.3 ± 16.7 mm^3; n = 16), PTT + DOX group (animals receiving PTT and free DOX, mean tumor size on day −1 = 135.9 ± 17.4 mm^3; n = 15) and Control group (animals not undergoing treatment, mean tumor size on day −1 = 135.8 ± 16.9 mm^3; n = 15). On this day, animals that would undergo PTT were injected with 190 µL NS intravenously. The following day, PTT, PTT + LIP and PTT + DOX groups underwent laser treatment as previously described.

Right after PTT, mice were injected intravenously with 40 µL of either free DOX (Teva Pharmaceuticals) or DOX-loaded liposomes (Doxil/Caelyx®, Janssen) at a concentration of 2 mg/mL of DOX in glucose solution (Fresenius Kabi, 100 mg/mL) to a final volume of 100 µL.

Statistics

Data are presented as mean ± standard error of the mean (SEM). One-way ANOVA and Tukey's post hoc test were used to compare the mean %ID/g of ^{64}Cu-loaded liposomes either at 10 minutes or 24 hours. A p value < 0.05 was considered significant. * represents $p < 0.05$, ** represents $p < 0.01$, and *** represents $p < 0.001$. The Kaplan–Meier method was used to create the survival curves, and these were compared with the Log-rank (Mantel-Cox) test. All data were plotted and analyzed on GraphPad Prism 9.

Results

In vivo Distribution of ^{64}Cu-Loaded Liposomes After Photothermal Therapy

First, we investigated whether NS-based PTT could enhance the uptake of liposomes in the tumor and at what time point after PTT this accumulation peaked. For this, we used ^{64}Cu-loaded liposomes with structural characteristics similar to those of the clinically approved PEGylated DOX-loaded liposomes and tracked their distribution in vivo via PET/CT imaging.

Mice bearing subcutaneous CT26 tumors were divided into four groups (n = 5 per group), where three of the groups received NS-based PTT (laser intensity of 1.5 W/cm^2 for five minutes) and were administered ^{64}Cu-loaded liposomes immediately (0 h group), 6 hours (6 h group), or 24 hours (24 h group) after therapy, respectively. The last group was administered ^{64}Cu-loaded liposomes without any PTT (control group). Using a thermal imaging camera, we confirmed that all three groups undergoing PTT had identical heating profiles, reaching a mean maximum temperature after five minutes of irradiation of 48.9 ± 1.2 °C (mean ± standard error of the mean (SEM)) in the 0 h group, 50.0 ± 0.9 °C in the 6 h group, and 49.9 ± 1.2 °C in the 24 h group (Figure 1A and B).

After PTT, ^{64}Cu-loaded liposomes were injected at the previously established timepoints. All animals were PET/CT scanned 10 minutes and 24 hours after the administration of liposomes, and the tumor uptake was quantified as the percentage of injected dose per gram of tissue (%ID/g) in 3D regions of interest (ROIs) created on entire tumors (Figure 1C). The mean tumor uptake of ^{64}Cu-loaded liposomes was significantly enhanced when the liposomes were administered immediately after therapy (0 h group). In contrast, there was no increase in tumor uptake when the liposomes were injected 6 hours after therapy or later (24 hours) in comparison to untreated

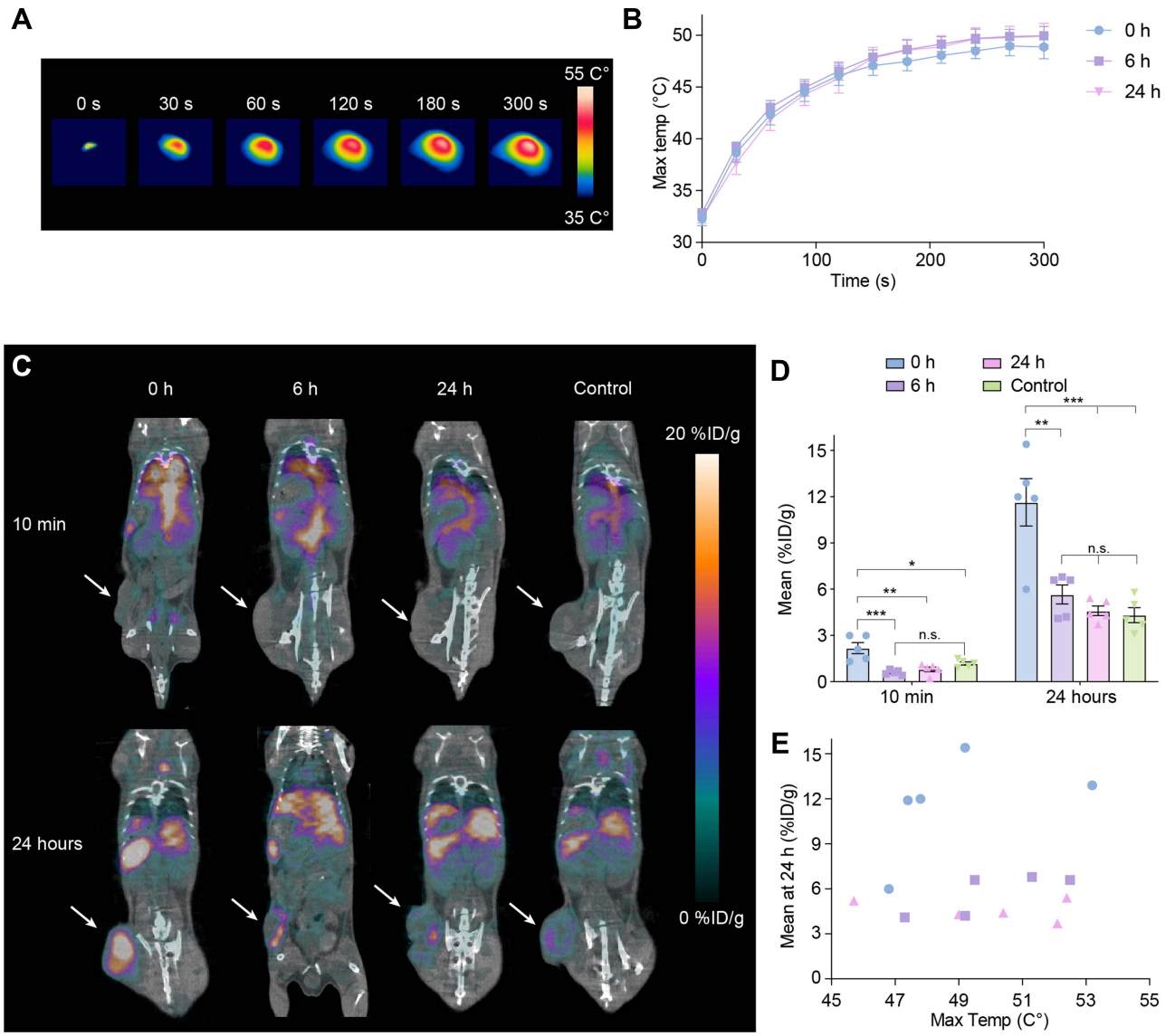

Figure 1 Distribution of ^{64}Cu-loaded liposomes after PTT in mice bearing CT26 tumors. (**A**). Representative images of a tumor at different time points during irradiation, captured with a thermal camera. (**B**). Temperature increase for all three groups of mice undergoing PTT, detected with the thermal camera (0 h, 6 h and 24 h). Data were shown as mean ± standard error of the mean (SEM). (**C**). Representative PET/CT images of mice 10 minutes and 24 hours after administration of ^{64}Cu-loaded liposomes. (**D**). Liposome accumulation in the tumor shown as mean percentage of injected dose per gram of tissue (%ID/g) for the different groups of mice (Control, 0 h, 6 h, and 24 h; n = 5 per group), 10 minutes and 24 hours after liposome administration. * represents $p < 0.05$, ** represents $p < 0.01$, and *** represents $p < 0.001$. n.s. means non-significant. (**E**). Correlation between the mean %ID/g (from the PET scans) and the maximum temperature reached during PTT (recorded with the thermal camera) for each mouse.

tumors (Figure 1D). Furthermore, the mean tumor uptake increased from 2.2 ± 0.4% ID/g at the 10-minute scan to 11.6 ± 1.5%ID/g at the 24-hour scan for the 0 h group, whereas the uptake increased only to 4–6% ID/g in the other groups.

To see if there was a positive trend between uptake and temperature, we plotted the mean tumor uptake of ^{64}Cu-loaded liposomes at the 24-hour scan as a function of maximum temperature reached for the individual animals (Figure 1E). In the 0 h group, it appeared that temperatures over 47 °C led to a drastic improvement in tumor uptake.

Ex vivo Distribution of DiI Fluorescent Liposomes in the Tumor After Photothermal Therapy

To study liposomal distribution within the tumor, fluorescently labeled DiI liposomes, resembling ^{64}Cu-loaded liposomes and the clinically approved DOX-loaded liposomes, were developed. We performed PTT on mice bearing CT26 tumors

and injected them with DiI liposomes right after laser treatment, the ideal timepoint for injection observed in the previous experiments with ^{64}Cu-loaded liposomes. An extra group of mice was injected with DiI liposomes without undergoing PTT. Mice were euthanized 24 hours after liposomal injection and tumors resected for ex vivo analysis.

First, we studied liposomal distribution in 20 μm tumor slices by detecting DiI fluorescence, and we could see a stronger fluorescent signal in tumors that had undergone PTT compared to tumors that did not undergo laser treatment (Figure 2A). This matched what we had observed for the ^{64}Cu-loaded liposomes, where PTT promoted liposomal accumulation in the tumor. Tumors from mice undergoing PTT but no liposomal injection were used as a control for unspecific staining.

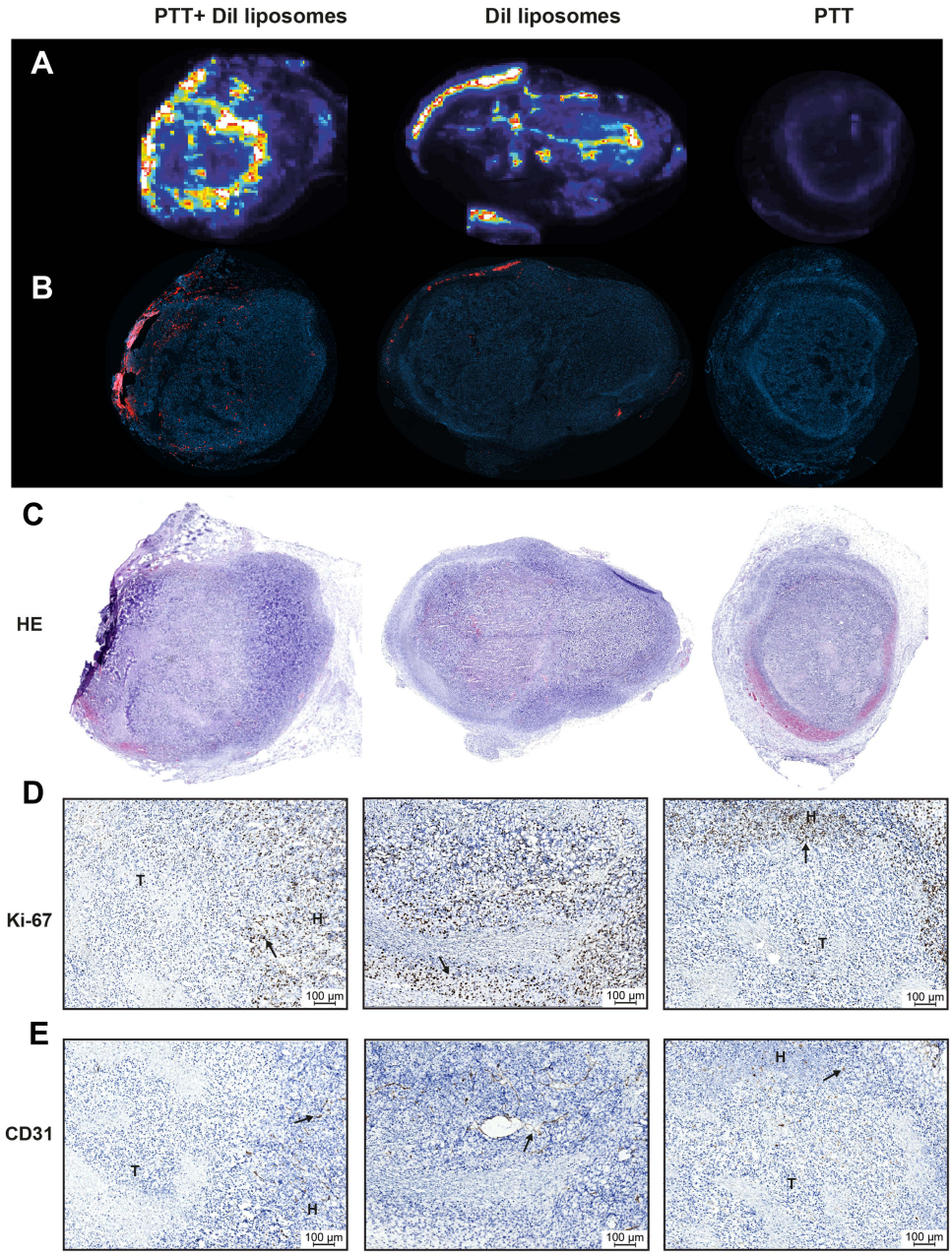

Figure 2 DiI liposomal distribution ex vivo in CT26 tumors and histological analysis. (**A**). Fluorescent DiI signal on 20 μm tumor slices for the different groups detected on the Amersham Typhoon Biomolecular Analyzer (n = 3). (**B**). Fluorescent signal on 4 μm tumor slices detected by microscopy. (**C**). HE staining. (**D**). Ki-67 staining. Arrows point to positive staining, denoted by brown color. T refers to treated tissue and H refers to healthy tissue. (**E**). CD31 staining.

We also studied fluorescence in 4 μm tissue slices through fluorescent microscopy for a more detailed view, and we observed that liposomes accumulated around the areas treated by the laser, which were determined by the absence of nuclei and confirmed through hematoxylin and eosin (HE) staining (Figure 2B and C). These areas consisting of dead or dying tissue were a result of the PTT.

Following, we confirmed that PTT-treated tumors presented with an absence of proliferating cells (Ki-67, Figure 2D) and reduced vascularity (CD-31, Figure 2E) in the treated areas.

Photothermal Therapy in Combination with Doxorubicin-Loaded Liposomes in vivo

After demonstrating that PTT improved liposomal delivery towards the tumor and determining the optimal injection timepoint to maximize the liposomal uptake (subsequently after PTT), we investigated the synergistic effect of NS-based PTT and DOX-loaded liposomes (Figure 3A). For this, CT26 tumor-bearing mice were divided into six groups: three of the groups were injected with NS and received PTT a day after NS injection; PTT group (PTT performed as a standalone treatment), PTT + DOX (PTT followed by injection of free DOX) and PTT + LIP (PTT followed by injection of DOX-loaded liposomes). Two additional groups were injected with either free DOX (DOX group) or DOX-loaded liposomes (LIP group), without undergoing PTT. The sixth group was the control group, not receiving any treatment.

Mice undergoing PTT (PTT, PTT + DOX, and PTT + LIP groups) were placed under the laser beam and treated for five minutes at 1.5 W/cm^2. The maximum temperatures reached on the tumor surface after five minutes of irradiation were comparable for all three groups (49.5 ± 1.3 °C in the PTT group, 48.3 ± 1 °C in the PTT + DOX group, and 50.2 ± 1.3 °C in the PTT + LIP group, Figure 3B). Right after laser treatment, PTT + DOX and PTT + LIP groups, along with DOX and LIP groups, were injected with 2 mg/mL of free DOX or DOX-loaded liposomes respectively, and tumor growth and survival (humane endpoints) were monitored for all groups. The study was terminated on day 60.

We observed that the combination of PTT + DOX-loaded liposomes (PTT + LIP group) led to a substantial slowdown in tumor growth and elongated survival when compared to all the other groups (Figure 3C–I). Two mice even experienced complete tumor regression, maintained until day 60. As for the other groups, there was a slight tendency of improved survival for PTT and PTT + DOX groups compared to the Control group. The outcome for DOX-loaded liposomes as a standalone treatment (LIP group) was very heterogeneous within the group and some of the mice benefited from the therapy, but the overall survival was significantly worse than when the liposomes were given in combination with PTT (LIP vs PTT + LIP; $p = 0.04$). The median survival was 13 days for the Control group, 15 days for the DOX group, 17 days for the PTT group, 15 days for the PTT + DOX group, 20 days for the LIP group, and 32.5 for the PTT + LIP group.

Discussion

The use of most current cancer therapeutics as standalone treatments is associated with several limitations, which has led researchers to focus on combination therapies to improve treatment outcome.[1] Traditional chemotherapy presents issues such as unspecific delivery of the drug, chemo-resistance, and potential cytotoxicity due to the high doses needed to elicit tumor death.[27–29] Nanoparticle-based PTT relies on light-induced hyperthermia to destroy cancer tissue, but it also fails to generate complete tumor regression due to, among other issues, the heterogeneous distribution of the heat, which leads to tumor recurrence arising from insufficiently heated areas.[30–32] We hypothesized that some of the limitations of chemotherapy and PTT as independent cancer treatments could be overcome with a dual approach. The rationale for this is the known abilities of hyperthermia to improve the accumulation of chemotherapeutic drugs in tumors and to potentiate their cytotoxic effect.[33,34] In addition, administering chemotherapy after PTT could assist in killing the residual cancer cells.[35] Accordingly, substantial effort has been put into combining PTT and chemotherapy. Multiple compounds have been developed to achieve all-in-one chemo-PTT compounds.[36–41] For example, Zheng et al[42] developed gold nanosponges loaded with DOX, achieving high therapeutic efficacy and minimal adverse effects in mice. DOX-loaded temperature-sensitive liposomes have also been developed. Here, the drug is released from the liposomes when irradiated with an appropriate source of light.[11,43] These approaches are very useful, but the treatment effect is generally observed where the chemo-PTT nanoparticle accumulates. We suggest that a treatment approach involving two separate treatments could elicit a more synergistic effect and have a higher likelihood of reaching a greater fraction of tumor cells.

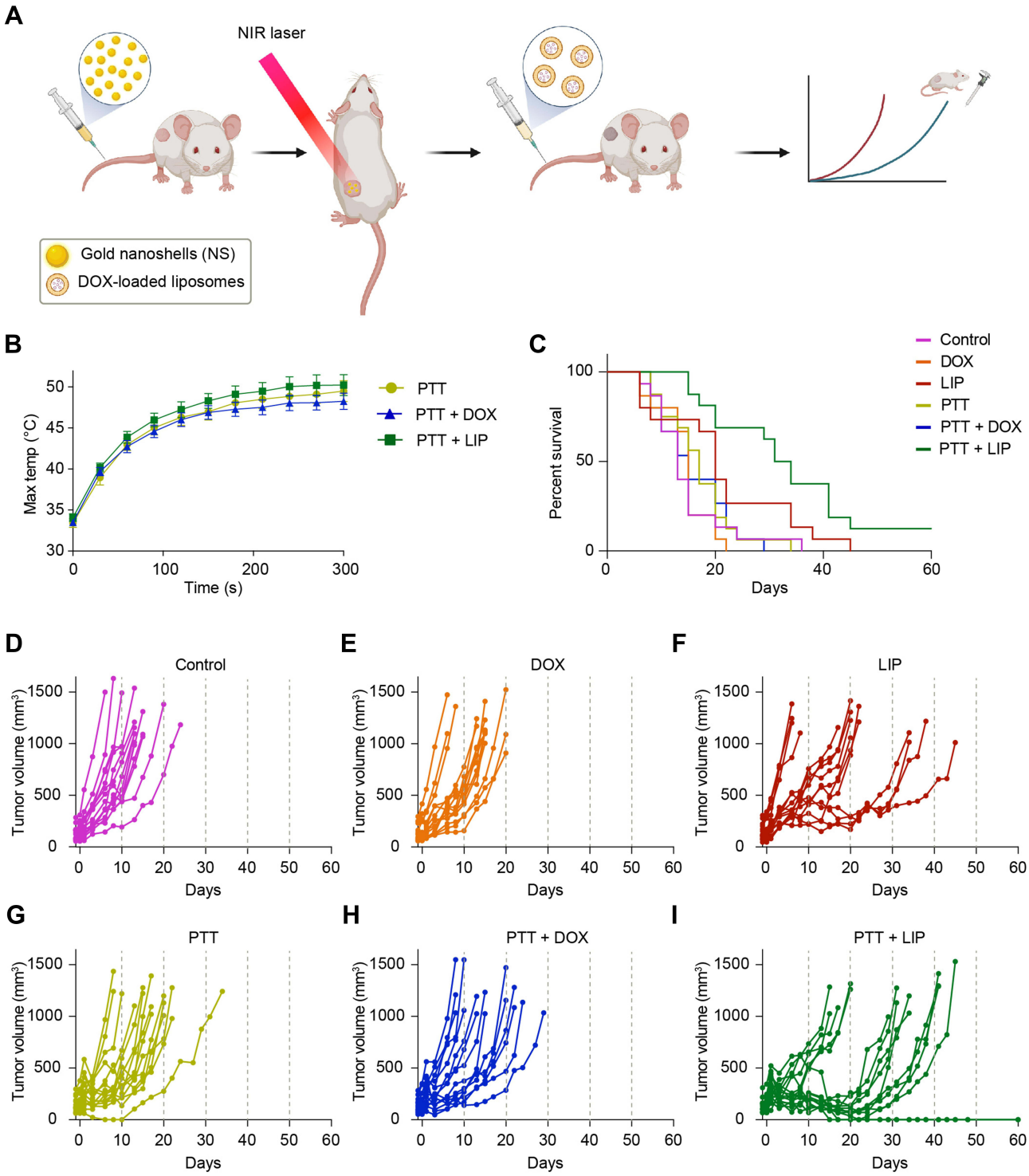

Figure 3 PTT as neoadjuvant treatment to DOX-loaded liposomes in mice bearing CT26 tumors. (**A**). Simplified timeline of the treatment schedule for mice undergoing combination treatment. Mice were injected with NS 24 hours before PTT. The following day, they were treated with the laser and immediately after they were injected with DOX-loaded liposomes. Tumor growth was followed by mechanical caliper measurements until endpoints were reached. Created with BioRender.com. (**B**). Temperature increase for all groups of mice undergoing PTT (PTT, PTT + DOX, and PTT + LIP), detected with a thermal camera. Data shown as mean ± SEM. (**C**). Survival curves for all groups included in the study; PTT (n = 16), LIP (n = 15), DOX (n = 15), PTT + LIP (n = 16), PTT + DOX (n = 15), and Control (n = 15). Study was terminated on day 60. (**D**–**I**). Growth curves for the individual mice in each of the groups.

Therefore, in the present study, we performed NS-based PTT followed by liposome administration in mice bearing subcutaneous CT26 colorectal tumors, a model frequently used for PTT and other in vivo cancer studies.[44–47] The optimal timepoint for liposomal administration after PTT was determined using ^{64}Cu-loaded liposomes and following their biodistribution through PET/CT imaging. The timing of the liposomal injection after PTT proved to be crucial since an increased accumulation of liposomes in the tumor was only achieved when these were administered immediately after the laser treatment, but not when PTT was performed 6 or 24 hours before the injection of liposomes. In addition, the use of fluorescent liposomes confirmed that tumor tissue from mice that had undergone PTT presented with higher liposomal accumulation when compared to non-treated tumors. The fluorescent signal was mainly seen in tumor regions adjacent to the ablated area, where the laser did not trigger cell death. This is most likely an effect of the milder hyperthermia occurring in these adjacent areas, which could be inducing a higher and more localized liposomal accumulation.

Finally, to evaluate the potential synergistic effect between PTT and administration of liposomal DOX, the treatment effect was evaluated in CT26 tumor-bearing mice. DOX-loaded liposomes were administered subsequently after PTT, and the tumor growth was followed over time. The treatment effect was compared to the one observed in mice receiving exclusively one of the treatments and a group receiving PTT and DOX in its free, non-encapsulated form. The combination of PTT and liposomal DOX led to a substantial slowdown in tumor growth and longer survival. These findings correspond well with our observation of PTT inducing an increase in liposome accumulation in the tumor. However, from our studies, it is not possible to determine if the improved treatment outcome is exclusively caused by this increase in uptake of liposomes or may also be due to other effects, such as the potentiation of the drug as a result of the hyperthermia triggered by PTT.

There are multiple points to consider when interpreting our findings; due to the multiple parameters involved in PTT (photosensitizer of choice and its biodistribution, laser power, location of the tumor, etc.), in-depth optimization of the treatment protocol would be needed before clinical translation.[10,32,48,49]

Also, even though some of the key toxicity issues related to the use of free DOX (or other traditional chemotherapeutics) are avoided when the drug is encapsulated, the liposomal formulations can trigger certain adverse effects in the patients (eg, hypersensitivity reactions, depletion of immune cells or triggering of inflammatory responses), which should be considered.[50,51] Another issue with current treatment regimens is the resistance to traditional chemotherapeutics. PTT is useful in this regard as it offers an alternative mechanism to generate cancer cell death, and so it would be advantageous to combine PTT with new non-traditional drugs, able to elicit tumor death through different mechanisms than those of traditional chemotherapeutics. For instance, it has previously been shown that successful chemo-PTT could be achieved by using chemical inhibitors of autophagy, which increase the susceptibility of the cancer cells to PTT-mediated killing.[52] Finally, both NS and liposomal DOX rely mainly on the EPR effect to reach and accumulate in the tumor. Apart from being extremely variable among tumor models, this passive targeting is often not enough to achieve a high therapeutic effect, and therefore tailored surface functionalization of nanocarriers to increase the anti-tumor effect and reduce toxicity is an important focus of research.[53–56] Furthermore, the EPR effect in humans is much more complex than previously thought, and it is also less pronounced than in mouse tumor models.[57,58] This should be assessed when considering nanotherapeutics for clinical translation. PTT could potentially help improve this EPR effect and should be studied further.

Conclusion

In conclusion, our studies show that the combination of neoadjuvant NS-based PTT and DOX-loaded liposomes inhibits tumor growth and improves survival in a mouse cancer model. This shows promise for NS-based PTT, a treatment already tested in human patients as a standalone therapy, since it could potentially be utilized as an add-on to other systemic cancer treatments.

Acknowledgments

The authors acknowledge the Core Facility for Integrated Microscopy, Faculty of Health and Medical Sciences, University of Copenhagen. Figure 3A and graphical abstract were created with Biorender.com.

Funding

This project received funding from the European Union's Horizon 2020 research and innovation programme under the grant agreements no. 670261 (ERC Advanced Grant) and 668532 (Click-It), the Lundbeck Foundation, the Novo Nordisk Foundation, the Innovation Fund Denmark, the Neuroendocrine Tumor Research Foundation, the Danish Cancer Society, the Arvid Nilsson Foundation, the Neye Foundation, the Research Foundation of Rigshospitalet, the Danish National Research Foundation (grant 126) - PERSIMUNE, the Sygeforsikringen "Danmark", the Research Council of the Capital Region of Denmark, the Danish Health Authority, the John and Birthe Meyer Foundation and the Research Council for Independent Research. Andreas Kjaer is a Lundbeck Foundation Professor.

Disclosure

The authors report no conflicts of interest in this work.

References

1. Mokhtari RB, Homayouni TS, Baluch N, et al. Combination therapy in combating cancer. *Oncotarget*. 2017;8(23):38022–38043. doi:10.18632/oncotarget.16723
2. Palmer AC, Sorger PK. Combination cancer therapy can confer benefit via patient-to-patient variability without drug additivity or synergy. *Cell*. 2017;171(7):1678–1691.e13. doi:10.1016/j.cell.2017.11.009
3. Nurgali K, Jagoe RT, Abalo R. Editorial: adverse effects of cancer chemotherapy: anything new to improve tolerance and reduce sequelae? *Front Pharmacol*. 2018;9:245. doi:10.3389/fphar.2018.00245
4. Eloy JO, Claro de Souza M, Petrilli R, Barcellos JPA, Lee RJ, Marchetti JM. Liposomes as carriers of hydrophilic small molecule drugs: strategies to enhance encapsulation and delivery. *Colloids Surf B Biointerfaces*. 2014;123:345–363. doi:10.1016/j.colsurfb.2014.09.029
5. Alavi M, Karimi N, Safaei M. Application of various types of liposomes in drug delivery systems. *Adv Pharm Bull*. 2017;7(1):3–9. doi:10.15171/apb.2017.002
6. Russell LM, Hultz M, Searson PC. Leakage kinetics of the liposomal chemotherapeutic agent Doxil: the role of dissolution, protonation, and passive transport, and implications for mechanism of action. *J Control Release*. 2018;269:171–176. doi:10.1016/j.jconrel.2017.11.007
7. Day ES, Morton JG, West JL. Nanoparticles for Thermal Cancer Therapy. *J Biomech Eng*. 2009;131:7. doi:10.1115/1.3156800
8. Riley RS, Day ES. Gold nanoparticle-mediated photothermal therapy: applications and opportunities for multimodal cancer treatment. *Wiley Interdiscip Rev Nanomed Nanobiotechnol*. 2017;9(4):e1449. doi:10.1002/wnan.1449
9. Kennedy LC, Bickford LR, Lewinski NA, et al. A new era for cancer treatment: gold-nanoparticle-mediated thermal therapies. *Small*. 2011;7(2):169–183. doi:10.1002/smll.201000134
10. Zhao L, Zhang X, Wang X, Guan X, Zhang W, Ma J. Recent advances in selective photothermal therapy of tumor. *J Nanobiotechnology*. 2021;19(1):335. doi:10.1186/s12951-021-01080-3
11. Yan F, Duan W, Li Y, et al. NIR-laser-controlled drug release from DOX/IR-780-loaded temperature-sensitive-liposomes for chemo-photothermal synergistic tumor therapy. *Theranostics*. 2016;6(13):2337–2351. doi:10.7150/thno.14937
12. Khan FA, Albalawi R, Pottoo FH. Trends in targeted delivery of nanomaterials in colon cancer diagnosis and treatment. *Med Res Rev*. 2022;42(1):227–258. doi:10.1002/med.21809
13. Gad SC, Sharp KL, Montgomery C, Payne JD, Goodrich GP. Evaluation of the toxicity of intravenous delivery of auroshell particles (gold–silica nanoshells). *Int J Toxicol*. 2012;31(6):584–594. doi:10.1177/1091581812465969
14. Stern JM, Kibanov Solomonov VV, Sazykina E, Schwartz JA, Gad SC, Goodrich GP. Initial evaluation of the safety of nanoshell-directed photothermal therapy in the treatment of prostate disease. *Int J Toxicol*. 2016;35(1):38–46. doi:10.1177/1091581815600170
15. Rastinehad AR, Anastos H, Wajswol E, et al. Gold nanoshell-localized photothermal ablation of prostate tumors in a clinical pilot device study. *Proc Natl Acad Sci USA*. 2019;116(37):18590–18596. doi:10.1073/pnas.1906929116
16. Amini SM. Gold nanostructures absorption capacities of various energy forms for thermal therapy applications. *J Therm Biol*. 2019;79:81–84. doi:10.1016/j.jtherbio.2018.12.007
17. Li Q, Chen K, Huang W, et al. Minimally invasive photothermal ablation assisted by laparoscopy as an effective preoperative neoadjuvant treatment for orthotopic hepatocellular carcinoma. *Cancer Lett*. 2021;496:169–178. doi:10.1016/j.canlet.2020.09.024
18. Gormley AJ, Larson N, Banisadr A, et al. Plasmonic photothermal therapy increases the tumor mass penetration of HPMA copolymers. *J Control Release*. 2013;166(2):130–138. doi:10.1016/j.jconrel.2012.12.007
19. Deng X, Shao Z, Zhao Y. Solutions to the drawbacks of photothermal and photodynamic cancer therapy. *Adv Sci*. 2021;8(3):2002504. doi:10.1002/advs.202002504
20. Nair RK, Christie C, Ju D, et al. Enhancing the effects of chemotherapy by combined macrophage-mediated photothermal therapy (PTT) and photochemical internalization (PCI). *Lasers Med Sci*. 2018;33(8):1747–1755. doi:10.1007/s10103-018-2534-5
21. Schaaf L, Schwab M, Ulmer C, et al. Hyperthermia synergizes with chemotherapy by inhibiting PARP1-dependent DNA replication arrest. *Cancer Res*. 2016;76(10):2868LP–2875. doi:10.1158/0008-5472.CAN-15-2908
22. Mendes R, Pedrosa P, Lima JC, Fernandes AR, Baptista PV. Photothermal enhancement of chemotherapy in breast cancer by visible irradiation of gold nanoparticles. *Sci Rep*. 2017;7(1):10872. doi:10.1038/s41598-017-11491-8
23. Mortezaee K, Narmani A, Salehi M, et al. Synergic effects of nanoparticles-mediated hyperthermia in radiotherapy/chemotherapy of cancer. *Life Sci*. 2021;269:119020. doi:10.1016/j.lfs.2021.119020
24. Barenholz Y. Doxil® — the first FDA-approved nano-drug: lessons learned. *J Control Release*. 2012;160(2):117–134. doi:10.1016/j.jconrel.2012.03.020

25. Kristensen K, Engel TB, Stensballe A, Simonsen JB, Andresen TL. The hard protein Corona of stealth liposomes is sparse. *J Control Release*. 2019;307:1–15. doi:10.1016/j.jconrel.2019.05.042
26. Ringgaard L, Melander F, Eliasen R, et al. Tumor repolarization by an advanced liposomal drug delivery system provides a potent new approach for chemo-immunotherapy. *Sci Adv*. 2022;6(36):eaba5628. doi:10.1126/sciadv.aba5628
27. Longley DB, Johnston PG. Molecular mechanisms of drug resistance. *J Pathol*. 2005;205(2):275–292. doi:10.1002/path.1706
28. Panda M, Biswal BK. Cell signaling and cancer: a mechanistic insight into drug resistance. *Mol Biol Rep*. 2019;46(5):5645–5659. doi:10.1007/s11033-019-04958-6
29. Cao L, Zhu Y, Wang W, Wang G, Zhang S, Cheng H. Emerging nano-based strategies against drug resistance in tumor chemotherapy. *Front Bioeng Biotechnol*. 2021;9. doi:10.3389/fbioe.2021.798882
30. Chatterjee DK, Diagaradjane P, Krishnan S. Nanoparticle-mediated hyperthermia in cancer therapy. *Ther Deliv*. 2011;2(8):1001–1014. doi:10.4155/tde.11.72
31. Chu KF, Dupuy DE. Thermal ablation of tumours: biological mechanisms and advances in therapy. *Nat Rev Cancer*. 2014;14(3):199–208. doi:10.1038/nrc3672
32. Simón M, Nørregaard K, Jørgensen JT, Oddershede LB, Kjaer A. Fractionated photothermal therapy in a murine tumor model: comparison with single dose. *Int J Nanomedicine*. 2019;14:5369–5379. doi:10.2147/IJN.S205409
33. Cao J, Chen Z, Chi J, Sun Y, Sun Y. Recent progress in synergistic chemotherapy and phototherapy by targeted drug delivery systems for cancer treatment. *Artif Cells Nanomed Biotechnol*. 2018;46(sup1):817–830. doi:10.1080/21691401.2018.1436553
34. Yang SJ, Huang CH, Wang CH, Shieh MJ, Chen KC. The synergistic effect of hyperthermia and chemotherapy in magnetite nanomedicine-based lung cancer treatment. *Int J Nanomedicine*. 2020;15:10331–10347. doi:10.2147/IJN.S281029
35. Luo D, Carter KA, Miranda D, Lovell JF. Chemophototherapy: an emerging treatment option for solid tumors. *Adv Sci*. 2017;4(1):1600106. doi:10.1002/advs.201600106
36. Xing S, Zhang X, Luo L, et al. Doxorubicin/gold nanoparticles coated with liposomes for chemo-photothermal synergetic antitumor therapy. *Nanotechnology*. 2018;29(40):405101. doi:10.1088/1361-6528/aad358
37. Li D, Zhang M, Yao J, Zhang Z. Rapid release from near-infrared polymer loaded liposomes for photothermal and chemo-combined therapy. *N J Chem*. 2019;43(5):2274–2277. doi:10.1039/c8nj04778b
38. Koga K, Tagami T, Ozeki T. Gold nanoparticle-coated thermosensitive liposomes for the triggered release of doxorubicin, and photothermal therapy using a near-infrared laser. *Colloids Surf a Physicochem Eng Asp*. 2021;626:127038. doi:10.1016/j.colsurfa.2021.127038
39. Yafout M, Ousaid A, Khayati Y, El Otmani IS. Gold nanoparticles as a drug delivery system for standard chemotherapeutics: a new lead for targeted pharmacological cancer treatments. *Sci Afr*. 2021;11:e00685. doi:10.1016/j.sciaf.2020.e00685
40. Karimi Zarchi AA, Amini SM, Salimi A, Kharazi S. Synthesis and characterisation of liposomal doxorubicin with loaded gold nanoparticles. *IET Nanobiotechnol*. 2018;12(6):846–849. doi:10.1049/iet-nbt.2017.0321
41. Aldahhan R, Almohazey D, Khan FA. Emerging trends in the application of gold nanoformulations in colon cancer diagnosis and treatment. *Semin Cancer Biol*. 2022;86:1056–1065. doi:10.1016/j.semcancer.2021.11.008
42. Zheng T, Li GG, Zhou F, Wu R, Zhu JJ, Wang H. Gold-nanosponge-based multistimuli-responsive drug vehicles for targeted chemo-photothermal therapy. *Adv Mater*. 2016;28(37):8218–8226. doi:10.1002/adma.201602486
43. You J, Zhang P, Hu F, et al. Near-infrared light-sensitive liposomes for the enhanced photothermal tumor treatment by the combination with chemotherapy. *Pharm Res*. 2014;31(3):554–565. doi:10.1007/s11095-013-1180-7
44. Chao TC, Chan LC, Ju SY, et al. In vivo growth suppression of CT-26 mouse colorectal cancer cells by adenovirus-expressed small hairpin RNA specifically targeting thymosin beta-4 mRNA. *Cancer Gene Ther*. 2014;21(9):389–396. doi:10.1038/cgt.2014.43
45. Xi J, Da L, Yang C, et al. Mn2+-coordinated PDA@DOX/PLGA nanoparticles as a smart theranostic agent for synergistic chemo-photothermal tumor therapy. *Int J Nanomedicine*. 2017;12:3331–3345. doi:10.2147/IJN.S132270
46. Nam J, Son S, Ochyl LJ, Kuai R, Schwendeman A, Moon JJ. Chemo-photothermal therapy combination elicits anti-tumor immunity against advanced metastatic cancer. *Nat Commun*. 2018;9:1. doi:10.1038/s41467-018-03473-9
47. Simón M, Jørgensen JT, Norregaard K, Kjaer A. 18F-FDG positron emission tomography and diffusion-weighted magnetic resonance imaging for response evaluation of nanoparticle-mediated photothermal therapy. *Sci Rep*. 2020;10(1):7595. doi:10.1038/s41598-020-64617-w
48. Fernandes N, Rodrigues CF, Moreira AF, Correia IJ. Overview of the application of inorganic nanomaterials in cancer photothermal therapy. *Biomater Sci*. 2020;8(11):2990–3020. doi:10.1039/D0BM00222D
49. Simón M, Jørgensen JT, Melander F, Andresen TL, Christensen A, Kjaer A. Photothermal therapy as adjuvant to surgery in an orthotopic mouse model of human fibrosarcoma. *Cancers*. 2021;13:22. doi:10.3390/cancers13225820
50. Fukuda A, Tahara K, Hane Y, et al. Comparison of the adverse event profiles of conventional and liposomal formulations of doxorubicin using the FDA adverse event reporting system. *PLoS One*. 2017;12(9):e0185654. doi:10.1371/journal.pone.0185654
51. Inglut CT, Sorrin AJ, Kuruppu T, et al. Immunological and toxicological considerations for the design of liposomes. *Nanomaterials*. 2020;10(2):190. doi:10.3390/nano10020190
52. Zhang Y, Sha R, Zhang L, et al. Harnessing copper-palladium alloy tetrapod nanoparticle-induced pro-survival autophagy for optimized photothermal therapy of drug-resistant cancer. *Nat Commun*. 2018;9(1):4236. doi:10.1038/s41467-018-06529-y
53. Shen S, Tang H, Zhang X, et al. Targeting mesoporous silica-encapsulated gold nanorods for chemo-photothermal therapy with near-infrared radiation. *Biomaterials*. 2013;34(12):3150–3158. doi:10.1016/j.biomaterials.2013.01.051
54. Chen F, Cai W. Nanomedicine for targeted photothermal cancer therapy: where are we now? *Nanomedicine*. 2015;10(1):1–3. doi:10.2217/nnm.14.186
55. Xia B, Wang B, Shi J, et al. Photothermal and biodegradable polyaniline/porous silicon hybrid nanocomposites as drug carriers for combined chemo-photothermal therapy of cancer. *Acta Biomater*. 2017;51:197–208. doi:10.1016/j.actbio.2017.01.015
56. Sonju JJ, Dahal A, Singh SS, et al. A pH-sensitive liposome formulation of a peptidomimetic-Dox conjugate for targeting HER2 + cancer. *Int J Pharm*. 2022;612:121364. doi:10.1016/j.ijpharm.2021.121364
57. Wilhelm S, Tavares AJ, Dai Q, et al. Analysis of nanoparticle delivery to tumours. *Nat Rev Mater*. 2016;1(5):16014. doi:10.1038/natrevmats.2016.14
58. Shi Y, van der Meel R, Chen X, Lammers T. The EPR effect and beyond: strategies to improve tumor targeting and cancer nanomedicine treatment efficacy. *Theranostics*. 2020;10(17):7921–7924. doi:10.7150/thno.49577